LAWRENCE
LIVERMORE
NATIONAL
LABORATORY

UCRL-JRNL-204649

Generation of Electric and Magnetic Fields During Detonation of High Explosive Charges in Boreholes

Sergey P. Soloviev, Jerry J. Sweeney

June 1, 2004

To be submitted to the Journal of Geophysical Research

DISCLAIMER

This work was performed under the auspices of the U.S. Department of Energy by University of California, Lawrence Livermore National Laboratory under Contract W-7405-Eng-48.

Generation of electric and magnetic fields during detonation of high explosive charges in boreholes

S.P. Soloviev

Institute of Geospheres Dynamics, Moscow, Russia

J.J. Sweeney

Lawrence Livermore National Laboratory, Livermore, CA, USA

Abstract

We present experimental results of a study of electromagnetic field generation during underground detonation of high explosive charges in holes bored in sandy loam and granite. Test conditions and physico-mechanical properties of the soil exert significant influence on the parameters of electromagnetic signals generated by underground TNT charges with masses of 2 – 200 kg. The electric and magnetic field experimental data are satisfactorily described by an electric dipole model with the source embedded in a layered media.

1. Introduction

Experimentalal studies of electromagnetic effects from chemical explosions show that electric and magnetic field signals are observed when explosions occur in the air, at the ground surface, and underground [*Adushkin and Soloviev*, 1996; *Boronin et al.*, 1990; *Martner and Sparks*, 1959; *Soloviev et al*., 2002; *Sweeney*, 1989; *Sweeney*, 1994; *Tomizawa and Yamada*, 1995]. The references cited above include observations of signals from underground nuclear explosions as well as chemical explosions. In one case [*Sweeney*, 1996] a comparison of nu-

clear and chemical explosions of similar energy in similar media indicated that low frequency electromagnetic signals are significantly larger for nuclear explosions, thus suggesting a possible exploitation of this phenomenon for discrimination under a nuclear test monitoring regime. Clearly, different source physical mechanisms come into play between underground nuclear and chemical explosions. In the nuclear case, the energy density and temperatures are much higher and gamma radiation interacting with the surrounding media produces a high flux of Compton electrons [*Wouters*, 1989]. Existing field data acquired from underground nuclear explosions and large underground chemical explosions has been obtained under relatively uncontrolled conditions, with a limited number of sensors with widely varying characteristics (frequency bandbass, sensitivity, sampling rate, etc.). The results of these field measurements show some general consistency, but we are very far from being able to make conclusions about source mechanisms for both underground nuclear and underground chemical explosions. For the case of well-controlled experiments, the characteristics of signals recorded for explosions above the surface, on the ground surface, and underground, respectively, show fundamental differences [*Soloviev et al.*, 2002; *Soloviev*, 2002; *Soloviev*, 2003]. The purpose of our experiments is to try to gain a better understanding of the generation electromagnetic fields during underground chemical explosions with well-controlled conditions.

Research to date in the field as well as the laboratory [*e.g. Dickinson et al., 1981; Brady and Rowell, 1986; Cress et al., 1987; Yamada et al., 1989; Chen et al., 1990, Enomoto and Hashimoto, 1990; O'Keefe and Thiel, 1991; O'Keefe and Thiel, 1995*] has shown that detonation of high explosive charges and fracture of rock are accompanied by a variety of electromagnetic effects attributed to a variety of physical causes. At an initial stage of an explosion it is possible to identify at least three processes connected to the generation of an elec-

tric and magnetic field: 1) propagation of a detonation wave through the explosive, 2) movement of explosion products and 3) propagation of a shock wave in the surrounding media. Each of these processes makes a contribution to the generation of electromagnetic signals that are observed. It is also necessary to take into account electrical currents that arise within the surrounding conductive media that occur as result of the interaction of shock waves and rock or soil.

Tomizawa and Yamada [1995] analyzed possible generation mechanisms of electric signals generated by three underground chemical explosions from measurements of the radial electric field, E_r, in the soil. In their experiments the explosive was placed along the length of the borehole, so these charges are not strictly a point source. All observations were made with instruments having a frequency response from 1 Hz to 5 kHz. Tomizawa and Yamada noted that the signal waveforms were different in each of three experiments, but the records of E_r have common characteristics: 1) the signals arise practically immediately after the explosive detonation and last not longer than 10 ms; 2) the characteristic oscillation period of the signal is about 1 ms; and 3) the process of signal generation can be modeled by vertical electric dipole. However, Tomizawa and Yamada did not present a model of the electric signals nor an estimation of electric dipole moment.

The observations and analysis of Soloviev *et al.* (2002) showed that the electric and magnetic field signals from an explosion at the ground surface can be complex and, in some ways, not predictable. In this case, Soloviev *et al.* suggested that the source of the field is electric charges in the explosion products and ionized gas that are in non-symmetric motion within the explosion cloud. The electromagnetic field produced by the contact explosion initially has a quadrupole character with a radial, r, dependence of r^{-4} out to a critical radius, r_0,

and an r^{-3} dependence farther out, where a dipole field term predominates. The interplay of the quadrupole and dipole terms also means that the electric field component will show a sign reversal with distance. In addition, there is an azimuthal dependence which depends on the characteristics of the source, thus the specific location of minima in the field as a function of azimuth cannot be determined *a priori*.

Generation of electrical currents during the propagation of seismic waves in the ground should be attributed to a separate group of the electromagnetic phenomena - so-called coseismic phenomena. In this work we investigate only the signals of the electric and magnetic field arising immediately after a detonation of high explosive charge, which are not associated with propagation of seismic waves.

2. Experimental program and instrumentation

We carried out a series of experiments to investigate the generation of electric and magnetic fields from explosions in a borehole. The underground explosions took place at two experimental sites where the ground possessed quite different physico-mechanical properties: sandy loam and natural granite. Characteristics of the high explosive charges, ground surface beneath the charge and configuration of the sensors are listed in Table 1.

In order to avoid any possible signal contribution from electric detonators, we used the (nonelectric) cap and fuse method for detonation of explosive charges in our experiments [*Gorshunov et al.*, 1967; *Soloviev et al.*, 2002]. The detonating cap was initiated by the fire beam from a safety fuse and transmitted the detonation to the main charge by means of the detonating cord. Detonating caps of type KD-8C were used in the experiments.

For the sandy loam site, boreholes up to 21 m depth were drilled with a diameter of 0.11 m. The holes were above the water table; no standing water was observed. Soil water content by weight was about 8-19 percent at depths up to 15 m. Density of the soil particles was in the range of $2{,}6 \cdot 10^3$ to $2{,}7 \cdot 10^3$ kg/m^3. During the experiments with smaller charges (events 1 –10), an charge assembly of explosive mass C = 0.7 – 4 kg consisting of the high explosive charge together with the detonator and the safety fuse was lowered down the bore-hole. In order to place larger charges, with mass of C = 15 – 200 kg (events 11 – 16), cavities were created at the required depth by explosions and then the cavities were filled with flake TNT. A schematic of the emplacement of an explosive charge with mass of 200 kg (event 16) is shown in Figure 1a.

It should be noted that the depth of burst, W, listed in Table 1 corresponds to a contained explosion ($WC^{-1/3}$ = 2 – 2.5 mkg$^{-1/3}$), with the exception of several events where $WC^{-1/3}$ < 2 mkg$^{-1/3}$. For the experiments in the sandy loam, ejection of sand from the boreholes in all cases was not observed; there was only a slight heaving of the soil in the epicentral zone. For events 15 and 16 with the largest charges, venting of a small volume of explosion products to the atmosphere via cracks in the soil was observed 2 –10 s after detonation time.

To carry out the experiments in the granite, a massif of Rapakivi granite near the city of Vyborg, Russia, was chosen. In the massif, there are several types of rapakivi structures and chemical compositions [*Velikoslavinsky et al*., 1978; *Suominen*, 1991]. The largest part of the massif is composed of the vyborgit, a porphyrite rock containing phenocrysts of potassium feldspar of ovoid, spherical, or irregular form. Speed of P-wave propagation in the massif is approximately $4{,}1\text{-}6{,}4 \cdot 10^3$ m/s and the granite density is approximately $2{,}63\text{-}2{,}83 \cdot 10^3$ kg/m^3.

Holes with diameter 0.1 and 0.25 m were bored in the granite massif. Figures 1b and 1c present a typical schematic of the emplacement of the explosive assemblage in the borehole and a photo of the explosive assemblage before being lowering into the borehole. The high explosive charge was assembled from individual TNT blocks of mass 0.2 kg. The detonating cord is strapped to two of the upper blocks. The free end of the detonating cord with the detonator attached to it was located at a depth of 0.3-0.5 m from the granite (ground) surface. The explosive charge was detonated with a delay determined by the length of the detonating cord used in each experiment. Timing of the high explosive charge detonation was defined with the help of an optical sensor consisting of an optical cable about 50 m in length, photoreceiver, and amplifier. One of the optical cable ends was mounted next to the detonator. The light impulse of the explosion was converted to a rectangular electrical signal with duration ~1 s. The leading edge of this signal lasted approximately 10^{-6} s after the beginning of high explosive charge detonation.

Figure 1b shows that the borehole in granite was stemmed with sand. For safety, the sand was not tamped because of the presence of the detonation cord. In some cases we used a combined stemming of sand with concrete on top. For the experiments in granite, ejection of sand from the boreholes was observed after detonation time in all cases. On the basis of video recordings of the explosions we observed that the ejection of sand from the boreholes took place after the arrival of seismic waves and thus had no bearing on the prompt-time electromagnetic signals of interest here.

Three components of electric field, **E**, (vertical component of the electric field strength in air and two horizontal components in the soil) and three components of the magnetic induction field, **B,** were recorded during the experiments. Arrival of the seismic waves generated by

the explosion was registered by accelerometers placed on the ground next to the E- and B-field recording sites. Type 4170 B&K accelerometers and 2651 charge amplifier were used in our experiments. All electromagnetic sensors and the explosion epicenter were placed along a direct line passing from east to west. This line coincides with the *x*-axis reference used in the theoretical analysis below. The projections of vectors **E** and **B** will be positive if they coincide with the positive direction of *x, y,* and *z*-axes (refer to Fig. 6). All electromagnetic sensors were installed on the ground surface. Sand was piled on the magnetic sensors to reduce wind effects and minimize ground motion.

The vertical electric field sensors used are passive electric antennas connected to a sensitive instrumental amplifier and filters. These electrometers, designed for a frequency band of 1 Hz to 10 kHz, have three output terminals (connectors) with amplification factors in the ratio of 1:10:100. The most sensitive third terminal has a response of about 2500 – 2900 mV/(V/m). Combined use of all terminals provides registration of the electric field strength from at least 1mV/m to 2000V/m.

The horizontal electric field sensors consist of electrodes buried in the soil connected by 10-20 m of wire laid on the soil surface and connected to an amplifier and filter. These lines, which are designed for a frequency band of 1 Hz to 10 kHz, have three output terminals (connectors) with amplification factors in the ratio of 1:10:100. The coil-induction magnetometers for the three-component B-field measurements consist of a magnetic sensor, preamplifier, integrator, and amplifier and filter circuits. The coil, with a high μ-metal core and preamplifier, is placed in a cylindrical waterproof case which is connected to the electronic unit by a cable. The magnetometers, with a frequency pass band of 60 Hz to 1.5 kHz, have a response of about 20 mV/pT for peak amplification. A narrow-band rejecter filter is placed in

the magnetometers as well as in the electrometers to provide suppression of 50 Hz industrial (power line) noise. In some experiments we used additional magnetometers with pass band of 500 Hz up to 10 kHz and sampling frequency up to 50 kHz. Results of these experiments showed that the waveform of the electromagnetic signals did not change significantly when sampling frequency was increased from 20 kHz to 50 kHz.

A notebook computer was used to acquire and digitally store signals of the magnetic and electric field using a 14-bit analog-to-digital converter; the converter allows synchronous multi-channel input of analog signals at sampling rates up to 500 kHz per channel. The sampling frequency generally used was 20 kHz. Batteries provided a self-contained power supply for the acquisition system, sensors of the electric and magnetic fields, and accelerometers.

Experimental results

Figures 2-5 show representative records of the electric and magnetic field signals generated by the detonation of high explosive charges in the boreholes. We have chosen, from the events listed in Table 1, characteristic events that are discussed in detail below. Time in Figures 2-5 is measured from the start of the analog-to-digital converter and recording. We first consider the signals of the electric and magnetic field recorded during the experiments in sandy loam. Figure 2 shows representative records of the electric and magnetic field generated by the detonation of high explosive charge with mass of 200 kg (event 16 and event 15). Figure 2g shows records of the vertical component of the ground acceleration. The accelerometers were placed on the ground surface at distances 20 m from the epicenter. It is obvious from Figure 2g that no ground motion occurs at the sensors at the time the electromagnetic signals are observed.

Emplacement conditions of the explosive charges with mass of 200 kg for events 16 and 15 were approximately the same (Table 1). It is evident from the scheme shown in Figure 1a that the primary charge explodes with a delay with respect to the detonator activation. The detonation time of the ancillary charge is marked in Figure 2b by a vertical arrow “A” and corresponds to 0.05 s (the sampling frequency was 20 kHz) from start of the record. The ancillary charge (Figure 1a) is a high explosive charge (trotil-hexogen 50/50) with mass of 0.13 kg that was placed at the depth of 4 m for event 15 and at the depth of 3.8 m for event 16. The delay time is determined by the length of the detonating cord and it was approximately equal to 1.3 and 1.45 ms for the events 16 and 15, respectively. The arrow “B” on Figure 2 marks the signal connected with arrival of seismic-explosive waves from the ancillary charge. Seismic-explosive waves induced by the primary charge arrive later.

As evident from Figures 2 and 3, the intensity of the electric and magnetic field signals observed after detonation are greater than background. Signal-to-noise ratios of the recorded signals are given in Table 1. The signal-to-noise ratio is the ratio between the peak signal magnitude observed after the detonation time and the average magnitude of background pulsations. Compared to other experiments in the sandy loam, we can see that the greatest signal-to-noise ratios correspond to the events 16 and 15. It should be noted that the signal to noise ratio can be increased by mathematical processing of the data, but all the figures presented are initial records of the electromagnetic signals without any processing of the digital records.

Pulse signals induced by electric processes in the surface layer of the Earth's atmosphere, such as electric discharges and so on (generally known as tellurics) are common for records of the electric and magnetic field signals. An example of such a signal is marked by the arrow “C” in Figure 2. Since the sensitivity of the sensors used for measurements is very high,

the presence of such pulse signals with large amplitude (as in the case when storm-clouds pass within a few tens of kilometers) could seriously complicate interpretation of the experimental data.

It is seen from Figures 2 and 3 that the signals from the explosions are low-frequency in character. The oscillation period of the fields is equal to several milliseconds. Peak signal amplitude of the E_z component is about 0.065 and 0.025 V/m at the distance 5 m from epi-center for the event 15 and 16 correspondingly. Figure 3a – 3e show records of vertical and radial components of electric field at different distances from epicenter for event 16. In this case (Figure 3a – 3c and 3e) and in some other cases the vertical and radial components of electric field are similar to each other; they have the same rise time and number of quasi-periods. After detonation, the magnetic field signals are remarkable only on the record of the B_z component at a distance of 5 m from the borehole, as shown in Figure 2-IIa (event 15 - peak amplitude of the signal is about 25 pT, whereas it is impossible to find any disturbances at this distance for the event 16). At a distance of 10 m from the borehole no magnetic field disturbances are observed for both experiments.

Figure 3 presents, at expanded amplitude scale, the records of $E_z(t)$ for r equal to 5 m, 7.5 m, 10 m, and 20 m from the borehole (event 16). It is obvious that the electric field signals arise at the same time at all distances r. The records of the $E_z(t)$ for the event 15 and 16 shown in Figures 2 and 3 call our attention to the fact that the signal polarity changes sign when distance r increases up to 20 m. This type of field behavior is typical for the field of an electric dipole placed at depth h from the air-ground interface: the amplitude of the E_z component becomes equal to zero at distances $r \sim h$, and then it changes sign. We will further discuss the dependence of the amplitude of the electric field components with distance r later.

From the experimental records presented above it follows that the signals of the electric and magnetic field arise immediately after detonation of the primary charge. The signals appear simultaneously on the records of sensors installed at different distances from the borehole; thus the signals are due to the same source. For the experiments carried out in sandy loam, it is evident from Table 1 and Figures 2 and 3 that amplitudes of the signals of the electric and magnetic field are characterized by a small value of the signal-to-noise ratio, i.e. in most events the signal amplitudes are slightly above background. It should be noted that in this case the largest disturbances after detonation time are observed for the radial component of the electric field in the ground; they are characterized by relatively larger values of the signal-to-noise ratio on the records of the electric and magnetic field components.

A different type of behavior is observed in the experiments carried out in the granite massif. Figures 4 and 5 show representative records of the electromagnetic signals for the events 18, 20, and 28. Figure 1b presents a typical schematic of the positioning of the explosive assembly in the borehole. For event 18 the depth of burst, W, was equal to 3.5 m. In this case, the delay time of the primary charge detonation was approximately equal to 0.55 – 0.6 ms. Signals of the electric and magnetic fields arise practically immediately after the explosive charge detonation. The arrow “B” on Figure 4 marks arrival of the ground motion at the points where field sensors are installed. The velocity of seismic wave propagation calculated from the accelerometer records was about 4 km/s (Figure 4e). Magnetic field sensors begin to oscillate with some delay after the seismic wave arrival; in this case account must be taken of the fact that the magnetometers are installed in a sand pile on the granite surface and aren’t in direct contact with the rock massif. An accelerometer installed on the magnetometer body showed that the delay really exists.

It is obvious from Table 1 and from Figures 4 and 5 that magnitudes of the electromagnetic signals observed immediately after the detonation time are significantly larger than background – the signal-to-noise ratio is greater than ten for most of the events. In some cases the radial and tangential components of the magnetic field are similar to each other (Figure 4a-b). Thus during experiment 18 about six quasi-periods of the signal were registered on the records of B_r and B_θ components of the magnetic field within a period from 0.1006 to 0.103 s as shown in Figure 4a-b (so one period lasts about 0.4 s). The signal magnitude gradually decreases with time with its maximum equal to about 200 pT. In this experiment there are not so many oscillations on the records of the E_z component of the electric field as were observed on the records of the magnetic field. However, the rise time of the initial spike of the E_z component is about 0.2 ms; this is close to the rise time of the magnetic field signals (Figure 4). The amplitude of the E_z component is equal to about 2 V/m at distance of 5 m from the borehole, whereas the amplitude of the E_r component is greater than 6 mV/m at distance of 15 m from the borehole.

As shown in Table 1, the explosive mass, W, for events 18, 20, and 28 is practically the same, but the waveform and magnitude of the electromagnetic signals obtained at the same distances from the borehole differ considerably. So, in the cases of the underground explosions in the granite it is an open question whether or not the signals of the electric and magnetic fields recorded at one of the radial directions are repeatable. In contrast to this, in the case when explosions occur on the ground surface, the variability of the electric field magnitudes in the different experiments with the same mass of explosive is about 10% [*Soloviev et al.*, 2002]. It seems likely that test conditions (physico-mechanical properties and a coarsely

crystalline structure of the granite next to the borehole and so on) exert significant influence on the parameters of electromagnetic signals generated by underground explosions.

Figure 4 shows $E_z(t)$ recorded at different distances, r, from the borehole for event 18: r equal to 5, 7.5, 10, and 12.5 m. Electric field signals arise at the same time at different distances, and signal polarity changes with distance just as it changes in the experiments in the sandy loam. Comparing the signals recorded during the sets of underground explosions in sandy loam and granite (the signals shown in Figures 2-5) is obvious that magnitudes of the signals of the electric and magnetic field for the explosions in granite recorded at the same distances are considerably larger. Moreover, it should be noted that the mass of the charges exploded in the sandy loam was 200 kg compared to a mass of only 2 kg for granite. However, the dependence on distance of E_z is similar for these two cases; signal polarity changes with distance from the borehole.

Theory

It is evident from the experimental data that underground detonation of high explosives is accompanied by electromagnetic phenomena. Formation and separation of electric charges and subsequent electric current generation in the ground cause the low-frequency electromagnetic field of an underground explosion. A detailed analysis of the electric and magnetic field generation, including all possible physics processes could be very difficult and is not the aim of this paper. However, in some cases the magnitude of possible sources can be estimated based on the experimental data. If the specific mechanisms of electromagnetic field generation are ignored, we can make an initial attempt to understand this phenomenon by envisioning the source as a point dipole.

We consider the case of an electric dipole in a conducting medium with a single horizontal interface. Components of the quasi-static field of the variable point dipole placed in a conductive half-space have been determined by [*Wait and Campbell*, 1958; *Wait*, 1961], but these analyses were done in the frequency domain, which is not convenient for interpreting time-domain experimental data. However, by considering the experimental conditions and making some assumptions and simplifications we can gain some useful insights. In the quasi-static case (when $\omega \to 0$) the formulas for the electric and magnetic fields can apply under the following conditions: $r << c/\omega$ and $r << (\mu_0 \gamma_1 \omega)^{-1/2}$, where r is distance from the field source to the measuring point, ω is radial frequency, μ_0 is the magnetic permittivity of free space, c is the velocity of light in free space, and γ_1 is ground conductivity. A second condition is connected with parameters characterizing the field diffusion in the conducting medium and is determined by the skin depth. It is obvious from the experimental data presented above that characteristic signal frequencies are not greater than 10^4 Hz. This second condition imposes more serious limitations than the first one: if $\gamma_1 = 5 \cdot 10^{-4} – 10^{-6}$ S/m (as in the case of the granite massif) then $r << 400 – 8800$ m, but if $\gamma_1 \approx 10^{-2}$ S/m (the sandy loam) then $r << 90$ m. We can see from Table 1 that all measurements were carried out within the near field of the source and the quasi-static approximation is valid for this case.

Therefore, the solution for the field produced by stationary point sources can be used to analyze low-frequency fields measured in the near field of the source. For example, it is known that in a uniform medium, the electric field of the variable electric dipole within the near zone ($r << c/\omega$) coincides with the field a static dipole of electric moment ($p = ql$),

[which is equal to the instantaneous value of the moment $p(t)$] and its magnetic field coincides with the field of an equivalent current element with length l (*Tamm*, 1976).

The situation where the stationary vertical and horizontal electric dipole is placed near the interface between two layers with conductivity γ_1 and γ_2 were analyzed by *Kaufman*, 1995. In his analysis, the electric dipole in the conductive medium is represented as a system of electric charges arising at two points with current flowing from one to the other. The total electric charge on the surface of the spherical current electrode placed in the uniform conductive medium with the specific resistance $\rho = 1/\gamma$ is equal to $q = \varepsilon_0 \rho I$, where I is the current arrived to the electrode [*Kaufman*, 1995]. The dipole moment is determined as $\mathbf{p} = \varepsilon_0 \rho I \, dl \, \mathbf{l}_0$, where $\mathbf{l}_0$ is unit vector showing the dipole moment direction.

A technique based on the simultaneous definition of the electric and magnetic fields was used to solve these problems [*Kaufman*, 1995]. If the calibration condition is written as

$$\text{div } \mathbf{A} = -\mu_0 \gamma U,$$

where $\gamma \neq 0$ and U is a scalar potential, the electric and magnetic fields can be expressed by means of only the vector potential $\mathbf{A}$:

$$\mathbf{E} = \frac{1}{\mu_0 \gamma} \text{grad div } \mathbf{A}, \qquad \mathbf{B} = \text{rot } \mathbf{A}. \tag{1}$$

The boundary condition is formulated and Laplace's equation for vector potential $\mathbf{A}$: $\nabla^2 \mathbf{A} = 0$, is solved for each of the problems.

We define a cylindrical coordinate system (r, θ, z) as shown in Figure 6 such that the dipole center coincides with the point of its origin and the z-axis is directed upward. In the case of the vertical electric dipole with moment $p_z = \varepsilon_0 \rho_1 I dz$, placed in the lower half-space, with conductivity γ_1 at the depth h from the boundary between two layers the vector potential will have only a vertical component A_z, whereas two other components A_r and A_θ will be

equal to zero. As a consequence the expression for the vector potential will be determined to be [*Kaufman*, 1995]:

$$A_{1z} = \frac{\mu_0 I dz}{4\pi R} - \frac{\mu_0 I dz}{4\pi}\frac{K_{12}}{R_1}, \qquad \text{if} \quad z \le h,$$

$$A_{2z} = \frac{\mu_0 I dz}{4\pi R}(1 - K_{12}), \qquad \text{if} \quad z \ge h,$$

where $K_{12} = \dfrac{\rho_2 - \rho_1}{\rho_2 + \rho_1}$ – a contrast coefficient which varies from −1 to 1, $\rho_1 = 1/\gamma_1$, $\rho_2 = 1/\gamma_2$, $R = \sqrt{r^2 + z^2}$, $\quad R_1 = \sqrt{r^2 + (2h - z)^2}$.

With equation (1) we can obtain the components of the electric and magnetic field. In the medium with conductivity γ_1 ($z \le h$) they will be:

$$E_{1z} = -\frac{\rho_1 I dz}{4\pi}\left(\frac{r^2 - 2z^2}{R^5} - K_{12}\frac{r^2 - 2(2h - z)^2}{R_1^5}\right), \quad E_{1r} = \frac{\rho_1 I dz}{4\pi}\left(\frac{3rz}{R^5} + K_{12}\frac{3(2h - z)r}{R_1^5}\right), \quad E_{1\theta} = 0,$$

$$B_{1z} = 0, \qquad B_{1r} = 0, \qquad B_{1\theta} = \frac{\mu_0 I dz}{4\pi}\left(\frac{r}{R^3} - K_{12}\frac{r}{R_1^3}\right). \tag{2}$$

In the medium with conductivity γ_2 ($z \ge h$) they will be:

$$E_{2z} = -\frac{\rho_2 I dz}{4\pi}(1 - K_{12})\frac{r^2 - 2z^2}{R^5}, \qquad E_{2r} = \frac{\rho_2 I dz}{4\pi}(1 - K_{12})\frac{3rz}{R^5}, \qquad E_{2\theta} = 0,$$

$$B_{2z} = 0, \qquad B_{2r} = 0, \qquad B_{2\theta} = \frac{\mu_0 I dz}{4\pi}(1 - K_{12})\frac{r}{R^3}. \tag{3}$$

In the case of the horizontal electric dipole placed at depth h from the boundary between two layers with the conductivity γ_1 and γ_2, as shown in Figure 6, the expressions for the components of the vector potential in a cylindrical coordinate system (r, θ, z) will be:

$$A_{1z} = -\frac{\mu_0 I dx}{4\pi} K_{12}\cos\theta\,\frac{R_1 - (2h - z)}{rR_1}, \qquad A_{1r} = \frac{\mu_0 I dx}{4\pi R}\cos\theta, \qquad A_{1\theta} = -\frac{\mu_0 I dx}{4\pi R}\sin\theta, \qquad \text{if } z \le h$$

$$A_{2z} = -\frac{\mu_0 I dx}{4\pi} K_{12}\cos\theta\,\frac{R - z}{rR}, \qquad A_{2r} = \frac{\mu_0 I dx}{4\pi R}\cos\theta, \qquad A_{2\theta} = -\frac{\mu_0 I dx}{4\pi R}\sin\theta, \qquad \text{if } z \ge h$$

where $R = \sqrt{r^2 + z^2}$, $R_1 = \sqrt{r^2 + (2h - z)^2}$. The components of the electric and magnetic field can be obtained from equation (1). In the medium with conductivity $\gamma_1 = 1/\rho_1$ ($z \le h$) they will be:

$$E_{1z} = \frac{(\varepsilon_0 \rho_1 I dx)3r\cos\vartheta}{4\pi\varepsilon_0}\left(\frac{z}{R^5} - K_{12}\frac{2h - z}{R_1^5}\right), \quad E_{1\theta} = \frac{(\varepsilon_0 \rho_1 I dx)\sin\theta}{4\pi\varepsilon_0}\left(\frac{1}{R^3} + K_{12}\frac{1}{R_1^3}\right),$$

$$E_{1r} = \frac{(\varepsilon_0 \rho_1 I dx)\cos\vartheta}{4\pi\varepsilon_0}\left[\frac{2r^2 - z^2}{R^5} + K_{12}\frac{2r^2 - (2h - z)^2}{R_1^5}\right]$$

$$B_{1z} = \frac{\mu_0 I dx}{4\pi}\frac{r\sin\theta}{R^3}, \qquad B_{1r} = \frac{\mu_0 I dx}{4\pi}\sin\theta\left[K_{12}\left(1 - \frac{2h - z}{R_1}\right)\frac{1}{r^2} - \frac{z}{R^3}\right], \tag{4}$$

$$B_{1\theta} = -\frac{\mu_0 I dx}{4\pi}\cos\vartheta\left[\frac{z}{R^3} + K_{12}\left(\frac{1}{r^2} - \frac{2h - z}{r^2 R_1} - \frac{2h - z}{R_1^3}\right)\right].$$

And in the medium with conductivity $\gamma_2 = 1/\rho_2$ ($z \ge h$) we have:

$$E_{2z} = \frac{(\varepsilon_0 \rho_1 I dx)\cos\vartheta}{4\pi\varepsilon_0}\frac{\rho_2}{\rho_1}(1 - K_{12})\frac{3zr}{R^5}, \quad E_{2r} = \frac{(\varepsilon_0 \rho_1 I dx)\cos\vartheta}{4\pi\varepsilon_0}\frac{\rho_2}{\rho_1}(1 - K_{12})\frac{2r^2 - z^2}{R^5},$$

$$E_{2\theta} = \frac{(\varepsilon_0 \rho_1 I dx)\sin\theta}{4\pi\varepsilon_0}\frac{\rho_2}{\rho_1}(1 + K_{12})\frac{1}{R^3}, \tag{5}$$

$$B_{2z} = \frac{\mu_0 I dx}{4\pi}\frac{r\sin\theta}{R^3}, \qquad B_{2r} = \frac{\mu_0 I dx}{4\pi}\sin\theta\left[K_{12}\left(1 - \frac{z}{R}\right)\frac{1}{r^2} - \frac{z}{R^3}\right],$$

$$B_{2\theta} = -\frac{\mu_0 I dx}{4\pi}\cos\vartheta\left[\frac{z}{R^3} + K_{12}\left(\frac{1}{r^2} - \frac{z}{r^2 R} - \frac{z}{R^3}\right)\right].$$

In the case of an arbitrarily-directed dipole, the electric and magnetic fields can be determined as a superposition of the fields of the vertical and horizontal dipole. The arbitrarily directed dipole placed in the soil at the depth *h* will be considered to be a source of the electric and magnetic field for the explosions in boreholes. Since sensors of the electric and magnetic fields are placed on the surface of the soil in the experiments, we can write the expressions for field components on the interface ($z = h$) of two layers: between the soil with the conductivity $\gamma_1 = 10^{-2} - 10^{-4}$ S/m and the air with the conductivity $\gamma_2 = 10^{-12} - 10^{-14}$ S/m. In this case con-

trast coefficient $K_{12} = \frac{\rho_2 - \rho_1}{\rho_2 + \rho_1}$ will be equal to $K_{12} \approx 1 - 2\rho_1/\rho_2$. It follows from equations (2) – (5) that the components of the electric and magnetic fields on the soil surface are presented as

$$E_z = \frac{p_z\left(2h^2 - r^2\right) + 3p_x hr\cos\theta}{2\pi\varepsilon_0 R^5}, \tag{6}$$

$$E_r = \frac{3p_z hr + p_x\left(2r^2 - h^2\right)\cos\theta}{2\pi\varepsilon_0 R^5}, \tag{7}$$

$$E_\theta = \frac{p_x \sin\theta}{2\pi\varepsilon_0 R^3}, \tag{8}$$

$$B_z = \frac{\mu_0 Idx}{4\pi}\frac{r\sin\theta}{R^3}, \tag{9}$$

$$B_r = \frac{\mu_0 Idx}{4\pi}\sin\theta\left(\frac{1}{r^2} - \frac{h}{r^2 R} - \frac{h}{R^3}\right), \tag{10}$$

$$B_\theta = -\frac{\mu_0 Idx}{4\pi}\cos\theta\left(\frac{1}{r^2} - \frac{h}{r^2 R}\right), \tag{11}$$

where $p_z = \varepsilon_0\, \rho_1\, I\, dz$, $p_x = \varepsilon_0\, \rho_1\, I\, dx$.

Components of the electric and magnetic fields E_r, E_θ, B_z, B_r, B_θ are continuous on the interface of two mediums, whereas the component E_z has a sudden change: $E_{1z} = E_{2z}\frac{\rho_1}{\rho_2} = E_{2z}\frac{\gamma_2}{\gamma_1}$. At the interface between the soil ($\gamma_1 = 10^{-2} – 10^{-4}$ S/m) and the atmosphere ($\gamma_2 = 10^{-12} – 10^{-14}$ S/m) E_{2z} component is ten orders higher than E_{1z} component, so here it is possible to neglect by the vertical component of the electric field in the soil.

Discussion

Parameters of the electric field source for the explosions in the borehole might be estimated on the basis of the records of $E_z(t)$, obtained at different distances r from the borehole at one of the radial directions, and from equation (6). For the chosen time moments after the detonation time we can determine three unknown parameters in equation (6): $\alpha_1(t) = \varepsilon_0\rho_1 Idz$, $\alpha_2(t) = (\varepsilon_0\rho_1 Idx)\cos\varphi$, and $\alpha_3(t) = h$ with the help of the least-squares method on the basis of

signal magnitudes measured by four (or more than four) electric field sensors placed at different distances from borehole. Equation (6) – (11) with calculated values of the parameters α_1, α_2, and α_3 allow interpolation of the time dependence of the electric and magnetic field at the different distances from the borehole. The computed results for events 16 and 18 are presented in Figures 3 and 4. It is apparent that equation (6) is a good approximation to the experimental data. Figures 3-h and 4-II-f show values of the component p_z and $p_x\cos\theta$ obtained from the model for the events 16 and 18, correspondingly.

Magnitudes of the radial component of the electric field, $E_r(t)$, calculated from equation (7) for the events in which E_r were measured, are a few times greater than the experimental values. However, the waveforms of calculated and experimental curves are nearly conformable. Thus Figure 3e gives the experimental and calculated curves for the explosion of the TNT charge with mass of 200 kg (event 16) at distance r = 20 m. At the instant of time t = 3.2 ms after the detonation time when the maximum magnitudes of the radial electric field are observed the ratio between the calculated and experimental magnitudes is about 4.

Equation (6) for the E_z component contains two terms. The first term is determined by the vertical component, p_z, and it decreases inversely with the cube of distance. The second term is determined by the horizontal component p_x and it decreases inversely proportional to the fourth power of distance. Moreover, the second term contains the cosine of the azimuth that leads to differences between the signal magnitudes in different directions. If $p_z = 0$ the signals at diametrically opposite directions have opposite polarities, but if $p_z > p_x$ or $r >> h$ the differences are not so distinct. As distance r from the explosion increases, behavior of the E_z component is mainly defined by the vertical component p_z of the dipole moment and a relationship between the signal magnitude and the azimuth is not significant.

As was the case for equation (6), the expression for the E_r component (equation (7) contains two terms. However, the first term decreases inversely proportional to the fourth power of distance and the second decreases inversely proportional to the cube of distance. As distance r from the explosion increases, the behavior of the E_r component is mainly defined by the horizontal component p_x of the dipole moment and a relationship between the signal magnitude and the azimuth becomes more and more significant.

Figure 3 presents the radial electric field, $E_r(t)$, calculated from equation (7) at distances of 20, 30, and 100 m from the charge for the event 16. The waveform of the signals changes with distance from the borehole because the second term in equation (7) decreases with distance more slowly than the first. Figure 7 shows the radial electric field, $E_r(t)$, calculated from equation (7) at distance r = 100 m for different azimuth, θ. It was assumed in the calculations that the estimate of the component $p_x\cos\theta$ derived above and shown in Figure 3h corresponds to θ =0°. It is obvious that the waveform of the signals changes with the azimuth: at the same instant of time the amplitudes of signals differ in values and in some cases in sign. For example, at the time t = 0,0532 s the ratio between the amplitudes of the signal $E_r(t)$ for θ = 0° and θ = 180° is about 4.

We can estimate components of the magnetic field on the basis of equations (9) – (11). Consider the records of the B_r and B_θ components obtained during the explosion with mass of 2 kg (event 18) and shown in Figures 4a-b. It is evident from the figures that the phases of the signals $B_r(t)$ and $B_\theta(t)$ are the same. Equations (10) and (11), for the B_r and B_θ components of the magnetic field, contain functions $\sin\theta$ and $\cos\theta$, correspondingly. In order for the phases of signals $B_r(t)$ and $B_\theta(t)$ to be the same, the azimuth θ must belong to the second quadrant ($90° \le \theta \le 180°$). For definiteness we shall use θ = 135°. With the parameters $\alpha_2(t)$ and $\alpha_3(t)$

obtained above on the basis of records of $E_z(t)$ at different distances r from the borehole we can calculate the estimates of $B_r(t)$ and $B_\theta(t)$. Computed results are presented in Figure 4a-b marked by a dotted line (specific resistance of the granite was used equal to $\rho_1 = 10^4$ Ohm-m). The curves show good correlation between the maximum amplitudes of the calculated and experimental signals of $B_r(t)$ and $B_\theta(t)$, but the waveforms of these signals are rather different.

Tomizawa and Yamada [1995] analyzed the radial component of electric field in the soil recorded during three explosions in a borehole. The mass of high explosive used in these experiments changed from 400 to 500 kg. For three events (Shot 3, Shot 4 and Shot 5) the magnitudes of the initial spike of radial electric field are presented in Table 2. The magnitudes of the initial spike calculated from equation (7) at distances of 30 and 100 m from the TNT charge with mass of 200 kg (events 15 and 16) are also presented in Table 2.

Hence Table 2 gives magnitudes of the initial spike of the radial electric field at distances of 30-100 m for five experiments. It is evident from comparison of the signal magnitudes that at distance of 100 m the magnitudes differ from each other by one or two orders of magnitude, whereas the explosive masses differ by 2-2.5 times. One might think that the differences in magnitude of the $E_r(t)$ signals might be caused by the azimuthal dependence. However, Figure 7 shows that the azimuthal dependence of the signal magnitudes suggests a ratio between the amplitude values of less than one order of magnitude. Evidently, some condition of the experiments, such as physico-mechanical properties of the soil where the explosion is carried out, exerts a more significant influence on the parameters of the field source.

Conclusion

The main results of this work are following:

1. Results of the experimental study show that for explosions of chemical charges in boreholes the signals of the electric and magnetic field arise immediately after the high explosive charge detonation and before the arrival of seismic waves to the points where the field sensors are installed. Three components of the electric field and three components of the magnetic field are observed after detonation time. Signals of the electric and magnetic field appear simultaneously on the records of the sensors placed at different distances from the borehole, which is to say that the signals are due to a single field source.

2. Behavior of the E_z component away from the borehole is the same for explosions in sandy loam as well as in granite at distances of 5 – 30 m, where signals were measured for our experiments: in both cases signal polarity changes with distance from the borehole.

3. We demonstrated that an electric dipole with two components, p_z and p_x, can be used to model the electric and magnetic field generated by an explosion in a borehole. The results obtained from the model and experimental data are in good agreement.

4. Comparing the signals recorded during sets of underground explosions in sandy loam and in granite, we see that amplitudes of the signals of the electric and magnetic fields recorded at the same distance are considerably greater for explosions in granite. Moreover, it should be noted that the mass of the charges exploded in the sandy loam was equal to 200 kg, whereas the mass of the charges exploded in the granite was only 2 kg. In the cases of the explosions in the sandy loam, the strongest disturbances are observed in the radial component of the electric field in the soil, which is characterized by relatively large values of the signal-to-noise ratio on the records of the electric and magnetic field components.

Estimates of the p_z and p_x components for the explosion of the TNT charge with mass of 2 kg carried out in the granite are more than an order of magnitude greater those for an analogous explosion in sandy loam.

5. Analysis of the electromagnetic signals obtained during the set of experiments with explosions in the boreholes shows that test conditions and, in particular, the physico-mechanical properties of the soil exert significant influence on the parameters of electromagnetic signals generated by underground explosions and on the parameters of the field source.

Acknowledgments

The work was performed with support of International Science and Technology Center grant number 2000;

References

Adushkin, V. V., and S. P. Soloviev, Generation of low-frequency electric fields by explosion crater formation, *J. Geophys. Res., 101*, 20,165-20,173, 1996.

Boronin, A. P., V. N. Kapinos, S. A. Krenev, and V. N. Mineev, On a physical mechanism of electromagnetic field generation by the explosion of condensed explosives charges: Literature review (in Russian), *The Physics of Combust. and Explosion, 26*, 110-116, 1990.

Brady, B. T., and G. A. Rowell, Laboratory investigations of the electrodynamics of rock fracture: *Nature, 1321*, 488-492, 1986.

Chen, B.-H., L.-H. Shi, and Y.M. Luo, A study of the geoelectric effects in the process of hydraulic fracturing experiments: *Acta Seismologica Sinica, 3,* 371-382, 1990.

Cress, G. O., B. T. Brady, and G. A. Rowell, Sources of electromagnetic radiation from frature of rock samples in the laboratory, *Geophysical Research Letters*, *14*, 331-334, 1987.

Dickinson, J. T., E. E. Donaldson, and M. K. Park, The emission of electrons and positive ions from fracture of materials, *Journal of Material Science, 16*, 2897-2908, 1981.

Enomoto, Y., and H. Hashimoto, Emission of charged particles from indentation fracture of rocks, *Nature, 346*, 641-643, 1990.

Gorshunov L. M., G. P. Kononenko, and E. I. Sirotinin, Electromagnetic disturbances under explosion, (in Russian), *J. Exp. Theoret. Phys., 53*, 818-821, 1967.

Kaufman A. A, Geophysical Field Theory and Method, Part A – Gravitational, electric and magnetic fields, International Geophysics Series, v. 49A-49C, Academic Press, San Diego, 1994.

Martner, S. T. and N. R. Sparks, The electroseismic effect, *Geophysics*, XXIV, 2, 297-308, 1959.

O'Keefe, S. G., and D. V. Thiel, Electromagnetic emissions during rock blasting, *Geophysical Research Letters, 18*, 889-892, 1991.

O'Keefe, S. G., and D. V. Thiel, A mechanism for the production of electromagnetic radiation during fracture of brittle materials, *Physics of the Earth and Planetary Interiors, 89*, 127-135, 1995.

Soloviev S. P., V. V. Surkov and J. J. Sweeney, Quadrupolar electromagnetic field from detonation of high explosive charges on the ground surface, *J. Geophys. Res., 107*, 10.1029/2001JB000296, 2002.

Soloviev S.P., Electric and magnetic field generated by the detonation of high explosive charges in the air and on the ground surface. (in Russian). *In Non-stationary processes in the uppermost and lowermost environments of the Earth, (Geophysics of large disturbances).* pp. 231-253, IDG RAS, Moscow, 2002.

Soloviev S.P. Generation of electric and magnetic field due to explosions in the borehole, (in Russian). *In Geophysical processes in the lowermost and uppermost environments of the Earth*, Part 1, pp. 249-267, IDG RAS, Moscow, 2003.

Suominen, V., The chronostratigraphy of south-western Finland with special reference to Postjotnian and Subjotnian diabases, *Bull. Geol. Surv. of Finland, 356,* 100 p., 1991.

Sweeney, J. J., An investigation of the usefulness of extremely low-frequency electromagnetic measurements for treaty verification, *Report UCRL-53899*, Lawrence Livermore Natl. Lab., Livermore, Ca, 1989.

Sweeney, J. J., Low-frequency electromagnetic measurements at the NPE and Hunter's Trophy: a comparison, in M. D. Denny, ed., *Proceedings of the Symposium on the Nonproliferation Experiment (NPE): Results and Implications for Test Ban Treaties,* U.S. Department of Energy report CONF-9404100, 8-21 to 8-33, 1994.

Sweeney, J. J., Low-frequency electromagnetic measurements as a zero-time discriminant of nuclear and chemical explosions, *Report UCRL-ID-126780*, Lawrence Livermore Natl. Lab., Livermore, Ca, 1995.

Tamm I.E., *Foundations of electricity theory* (in Russian), 616 pp., Nauka, Moscow, 1976.

Tomizawa I. and I. Yamada, Generation mechanism of electric impulses observed in explosion seismic experiments, *J. Geomag. Geoelectr., 47,* 313 – 324, 1995.

Velikoslavinsky D.A., A. P. Birkis, O. A. Bogaticov et al., *Anorthosite-rapakivi-granite formation* (in Russian), 296 pp., Nauka, Leningrad, 1978.

Wait J.R., and Campbell, L.L, The fields of an electric dipole in a semi-infinite conducting medium: *J. Geophys. Res., 58,* 1, 21-28, 1953.

Wait J.R., The electromagnetic fields of a horizontal dipole in the presence of a conducting half-space: *Can. J. Phys. 39*, 14, 1017-1028, 1961.

Wouters, L. F., The underground electromagnetic pulse: four representative models, Lawrence Livermore National Laboratory report UCID-21720, 20 pp., 1989.

Yamada, I. K., K. Masuda, and H. Mizutani, Electromagnetic and acoustic emission associated with rock failure, *Physics of the Earth and Planetary Interiors, 57*, 157-168, 1989.

Figures

Figure 1. Schematics of the borehole explosion experiment set-up. (a) Assembly of an explosive charge of mass of 200 kg (event 16) for detonation in sandy loam. (b) Assembly of an explosive charge of mass 2 kg for detonation in granite. (c) Photo of the explosive assembly (assembled from TNT blocks with mass of 0.2 kg) before being lowered down a borehole.

Figure 2. Electromagnetic signals recorded during explosions with mass of 200 kg (event 16, Figure 2-I; event 15, Figure 2-II). (a, b, c) Magnetic field components, $B_z(t)$, $B_r(t)$, $B_\theta(t)$ at 5 m distance from borehole, respectively, A: detonation time, B: time associated with arrival of seismic wave. (d, e, f) Vertical electric field component, $E_z(t)$, at 5 m, 7.5 m and 20 m distance from borehole, respectively, C: Telluric pulse signals, not associated with the explosion. (f) Vertical acceleration component at 20 m distance from borehole (note expanded time scale).

Figure 3. View with vertically expanded scale of electric field signals recorded during an explosion with mass of 200 kg (event 16). (a, b, c, d) Vertical electric field component, $E_z(t)$, at 5 m, 7.5 m, 10 m and 20 m distance from borehole, respectively, A: detonation time. $E_z(t)$ obtained from the model (equation (6)) is shown by dashed line. (e) Radial electric field component, $E_r(t)$, at 20 m distance from borehole. $E_r(t)$ obtained from the model (equation (7)) is shown by dashed line. (f, g) Radial electric field component, $E_r(t)$, at 30 m and 100 m distance from borehole obtained from the model (equation (7)). (h) Vertical and horizontal components, p_z, p_x, of the electric dipole moment versus time, curve 1: Vertical component, p_z, curve 2: Horizontal component, p_x.

Figure 4. Electromagnetic signals recorded during the explosion with mass of 2 kg (event 18). The right side set of figures are the same as the ones on the left, but with an expanded time scale. (a, b) Radial and tangential magnetic field components, $B_r(t)$, $B_\theta(t)$, at 5 m distance from borehole, respectively, $B_r(t)$, $B_\theta(t)$, obtained from the model (equation (10, 11)) is shown by dashed line. (c, d, e) Vertical electric field component, $E_z(t)$, at 5 m, 7.5 m and 10 m distance from borehole, respectively, $E_z(t)$ obtained from the model (equation (6)) is shown by dashed line. (I-f) Radial electric field component, $E_r(t)$, at 15 m distance from borehole. (I-g) Vertical acceleration component at 10 m distance from borehole. (II-f) Vertical electric field component, $E_z(t)$, at 12.5 m distance from borehole, $E_z(t)$ obtained from the model (equation (6)) is shown by dashed line. (II-g) Vertical and horizontal components, p_z, p_x, of the electric dipole moment versus time, curve 1: Vertical component, p_z, curve 2: Horizontal component, p_x.

Figure 5. Electromagnetic signals recorded during the explosion with mass of 2 kg.

(I) – event 20. (a, b) Vertical and radial magnetic field components, $B_z(t)$, $B_r(t)$, at 5 m distance from borehole. (c, d) Vertical electric field component, $E_z(t)$, at 5 m, and 7.5 m distance from borehole, respectively. (e) Radial electric field component, $E_r(t)$, at 13 m distance from borehole. (f) Vertical acceleration component at 10 m distance from borehole.

(II) – event 28. (a, b) Vertical magnetic field components, $B_z(t)$, at 5 m and 7.5 m distance from borehole, respectively. (c, d, e) Vertical electric field component, $E_z(t)$, at 5 m, 10 m and 15 m distance from borehole, respectively. (f) Radial electric field component, $E_r(t)$, at 15 m distance from borehole.

Figure 6. System of coordinates and plan of location of effective electric dipole used in the model to estimate electric and magnetic fields.

Figure 7. Radial electric field component, $E_r(t)$, obtained from the model (equation (7)) at 100 m distance from borehole for different azimuth θ (event 16).

(a) $\theta = 0°$. (b) $\theta = 45°$. (c) $\theta = 90°$. (d) $\theta = 135°$. (e) $\theta = 180°$.

Table 1. Explosions in the borehole – Characteristics of the high explosive charges, ground, emplacement of the sensors, and signal/noise ratio

Event	Mass of high expl., kg	Explo-sive	Ground	*W*, m	Emplacement of sensors					
					Electric field sensors			Magnetic field sensors		
					Distance *r*, m	Com-ponent	Signal/ noise	Distance *r*, m	Compo-nent	Signal/ noise
1	2,0	TH 50/50	sandy loam	1,9	7,5 11,3	E_z E_z	<2 <2	7,5 16,2	B_z, B_r, B_θ B_z, B_r, B_θ	5 2
2	2,0	TH 50/50	sandy loam	2,3	7; 14	E_z	<2	7; 14	B_z, B_r, B_θ	<2
3	2,0	TH 50/50	sandy loam	2,35	4 9	E_z E_z	<2 <2	4 4	B_z B_r, B_θ	5 <2
4	2,0	ammo-nite	sandy loam	2,3	5 10	E_z E_z	3 2	5 5	B_z B_r	10 4
5	0,7	TH 50/50	sandy loam	2,35	10	E_z	3	4 4	B_z, B_r B_θ	3 <2
6	2,0	TH 50/50	sandy loam	2,8	5 8	E_z E_z	2 <2	5 5	B_z B_r, B_θ	7 <2
7	2,0	TH 50/50	sandy loam	2,8	5	E_z	<2	5	B_z	2
8	2,05	TNT	sandy loam	2,95	5; 7,5; 10 12,5; 15	E_z E_z E_r	4-2 <2 3	5 10	B_z, B_r, B_θ B_z, B_r, B_θ	3 <2
9	4,05	ammo-nite	sandy loam	17,75	5 7,5	E_z E_z	<2 <2	5 5	B_z B_r, B_θ	2 <2
10	3,05	ammo-nite	sandy loam	15,55	5 7,5 15	E_z E_z E_r	4 <2 8	5 5	B_z B_r, B_θ	3 <2
11	20	TNT	sandy loam	6,3	5; 10,8	E_z	<2	10,8; 21,5	B_z, B_r, B_θ	<2
12	15	TNT	sandy loam	13,85	5; 10	E_z	<2	5	B_z, B_r, B_θ	<2
13	20	TNT	sandy loam	11,65	5; 10 15	E_z E_r	2 10	5	B_z, B_r, B_θ	<2
14	2,1	ammo-nite	sandy loam	2,9	5; 10 15	E_z E_r	2 3	5	B_z, B_r, B_θ	<2
15	200	TNT	sandy loam	14,3-12,6	5 7,5 10 20 20	E_z E_z E_z E_z E_r	6 4 2 2 10	5 5 10	B_z B_r, B_θ B_z, B_r, B_θ	7 <2 <2
16	200	TNT	sandy loam	15,2-13,4	5 7,5 10 20 20	E_z E_z E_z E_z E_r	10 5 3 5 10	5 10	B_z, B_r, B_θ B_z, B_r, B_θ	<2 <2
17	1,2	TNT	granite	1,35	5 – 12,5	E_z	>10	5	B_r, B_θ	>10
18	2,0	TNT	granite	3,5	5 – 12,5	E_z	>10	5	B_r, B_θ	>10
19	2,0	TNT	granite	2,75	5 – 12,5 17,8	E_z E_r	>10 8	5	B_z, B_r	>10
20	2,0	TNT	granite	3,3	5 – 12,5 13,05	E_z E_r	>10 >10	5	B_z, B_r	>10

Extension of Table 1.

Event	Mass of high expl., kg	Explo-sive	Ground	*W*, m	Emplacement of sensors					
					Electric field sensors			Magnetic field sensors		
					Distance *r*, m	Com-ponent	Signal/ noise	Distance *r*, m	Compo-nent	Signal/ noise
21	2,0	TNT	granite	3,37	5 – 12,5 15	E_z E_r	>10 >10	5	B_z, B_r	>10
22	10,4	TNT	granite	7,0	5 – 12,5 20	E_z E_r	>10 >10	5	B_z, B_r	>10
23	2,0	TNT	granite	7,55	5 7,5 10 12,5	E_z E_z E_z E_z	10 4 2 <2	5	B_z, B_r	5
24	2,0	TNT	granite	3,0	5,8 – 9,2	E_z	>10	5,8	B_z	>10
25	10,0	TNT	granite	5,1	7,5 – 10 20 – 30 20	E_z E_z E_r	>10 2 >10	7,5 –10 15 – 30	B_z B_z	>10 2
26	2,0	TNT	granite	5,2	5 7,5 10 – 19	E_z E_z E_z	5 2 <2	5 7,5 10 – 19	B_z B_z B_z	5 2 <2
27	2,0	TNT	granite	2,8	4 – 11,5 15,5 11,5	E_z E_z E_r	2 <2 2	4 6,5 – 11,5 15,5 – 21,5	B_z B_z B_z	10 2 <2
28	2,0	TNT	granite	3,5	5 – 17,5 15	E_z E_r	>10 >10	5 – 7,5 10 – 12,5 15	B_z B_z B_z	>10 10 7
29	2,0	TNT	granite	5,3	5 7,5 15	E_z E_z E_r	>10 5 5	5 7,5	B_z B_z	>10 >10
30	3	TNT	granite	3,3	10,7 – 23 20	E_z E_r	>10 >10	10,7 – 23	B_z	>10
31-32	0,4 0,4	TNT	granite	1,65 1,45	5 7,5 – 10,2 15	E_z E_z E_r	8 <2 3	5 7,5 10,2	B_z B_z B_z	10 2 <2
33	2,0	TNT	granite	4,65	5 7,5 – 17,5	E_z E_z	5 2	5 7,5 – 17,5	B_z B_z	10 5
34	2,0	TNT	granite	3,87	5 7,5 – 10	E_z E_z	5 2	5 7,5 – 15	B_z B_z	10 2

Table 2. magnitudes of initial spike of radial electric field at distances 30-100 m for five experiments.

Event	15		16		Shot 3		Shot 4	Shot 5
_, kg	200		200		450		400	500
W, m	13,4		14,3		54		42,5	42,5
L, m	1,7		1,8		42		35	45
r, m	30	100	30	100	30	100	125	100
E_r, μV/m	2000	30	1000	10	30	5	400	125

Figure 1

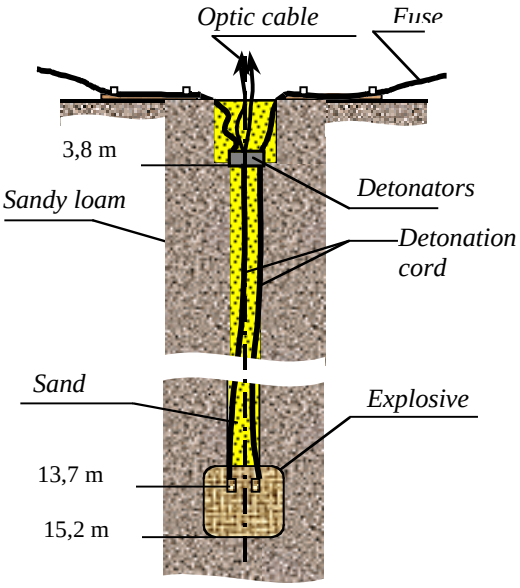
Optic cable
Fuse
3,8 m
Sandy loam
Detonators
Detonation cord
Sand
Explosive
13,7 m
15,2 m

a

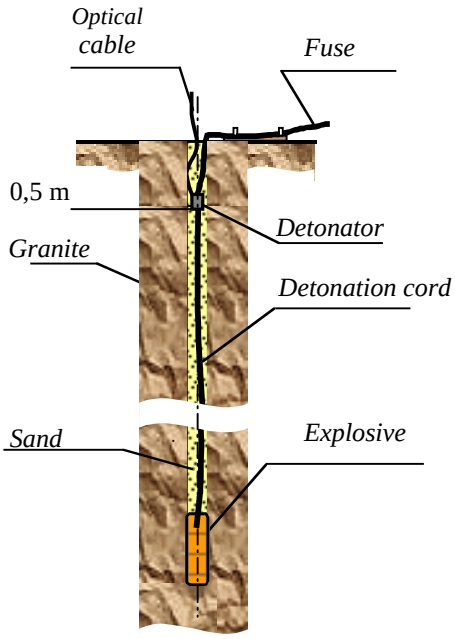
Optical cable
Fuse
0,5 m
Granite
Detonator
Detonation cord
Sand
Explosive

b

c

Figure 2

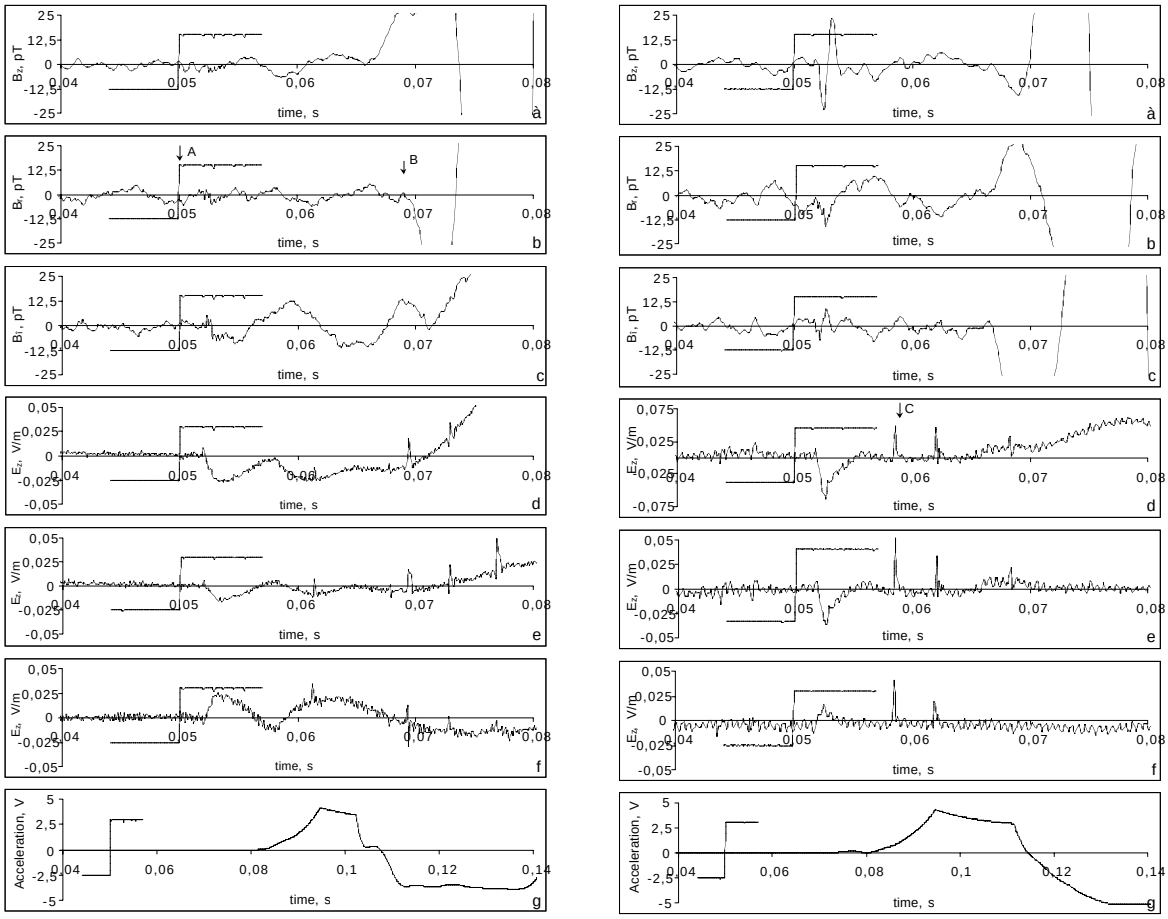

Figure 3

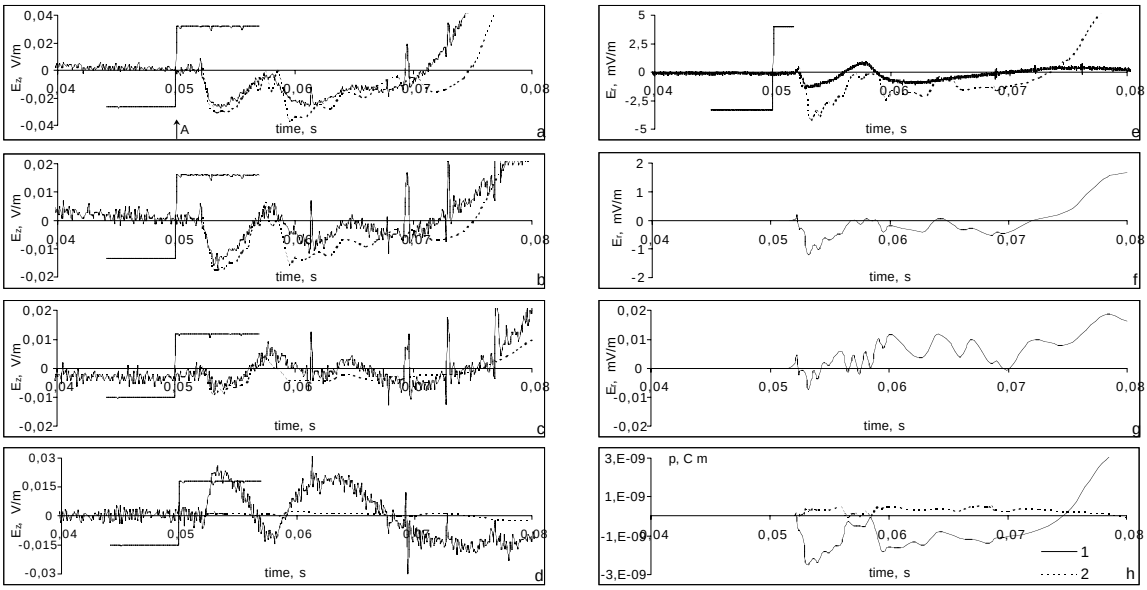

Figure 4

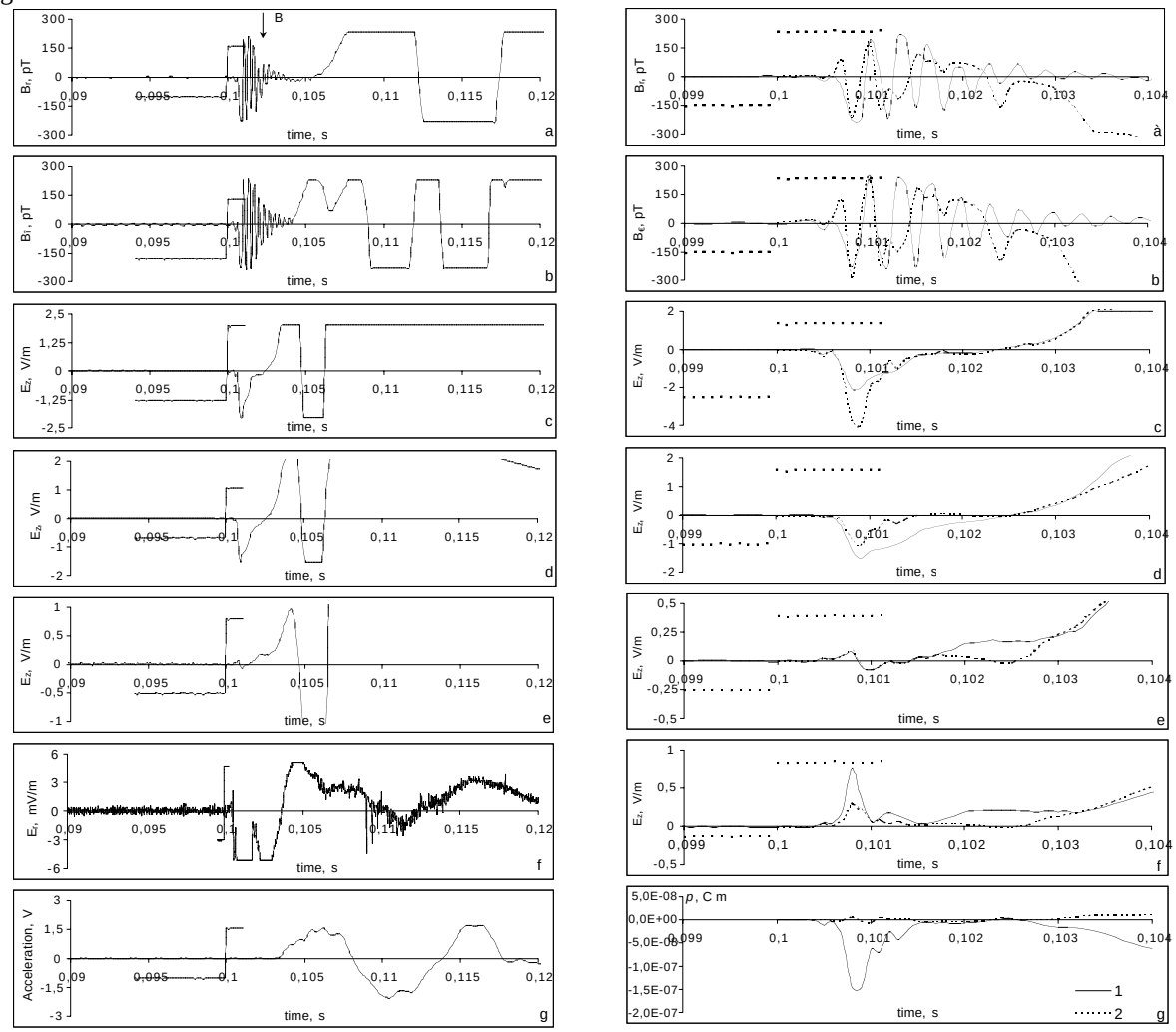

Figure 5

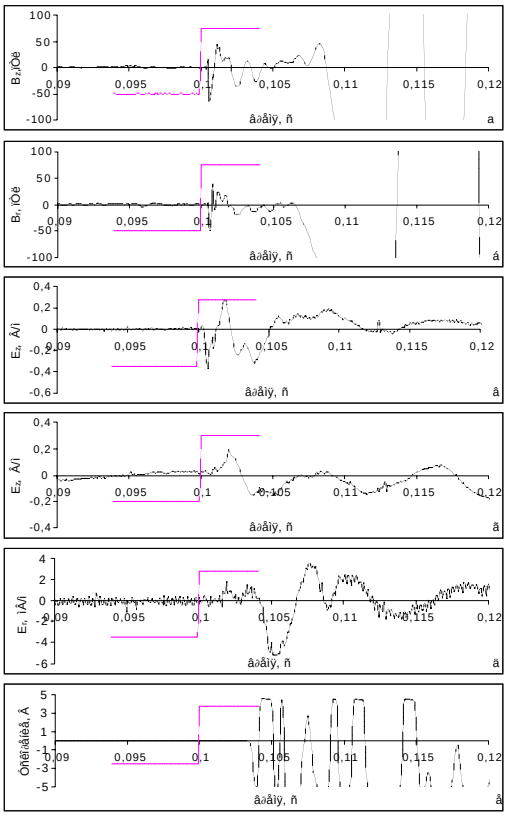
100
50
0
-50
-100
0,09
0,095
0,1
0,105
0,11
0,115
0,12
âòåìÿ, ñ
0,4
0,2
-0,2
-0,4
-0,6
0,5
0,3
-0,3
-0,5
4
2
-2
-4
-6
5
3
1
-1
-3
-5
1,5
-1,5

I

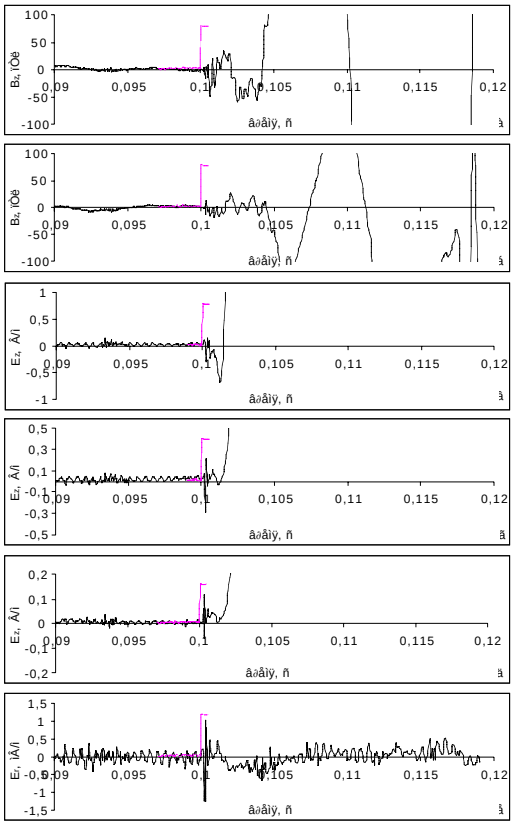
100
50
0
-50
-100
0,09
0,095
0,1
0,105
0,11
0,115
0,12
âòåìÿ, ñ
1
-1
0,5
-0,5
0,3
-0,3
0,2
-0,2
1,5
-1,5

II

Figure 6

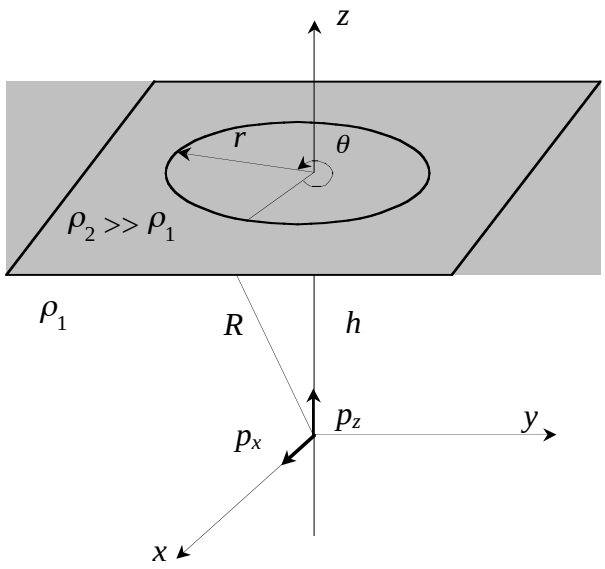

Figure 7

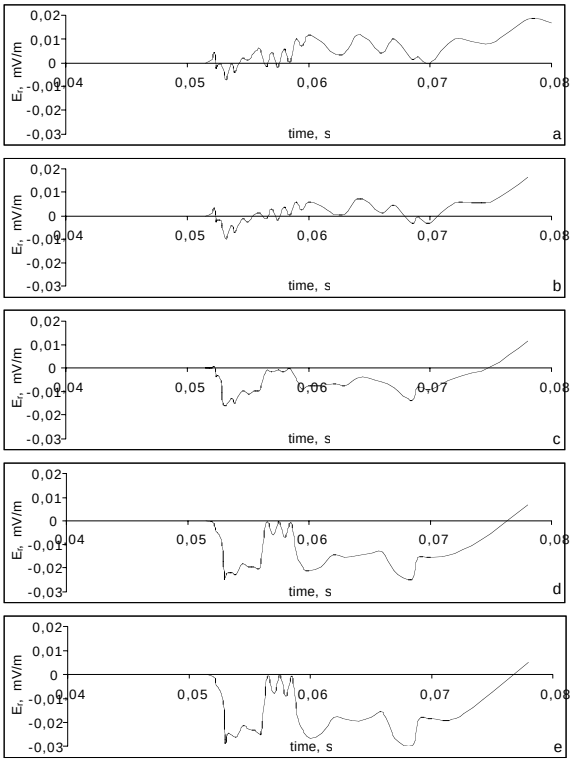

University of California
Lawrence Livermore National Laboratory
Technical Information Department
Livermore, CA 94551